Electronic Supplementary Material (ESI) for Journal of Materials Chemistry A.
This journal is © The Royal Society of Chemistry 2021

Supporting Information

Electrochemically induced structural reconstruction in promoting Zn storage performances of $CaMn_3O_6$ cathode for superior long life aqueous Zn-ion battery

Peisheng Guo[1], Gongzheng Yang[1], Chengxin Wang[1,2]*

[1]State Key Laboratory of Optoelectronic Materials and Technologies, School of Materials Science and Engineering, Sun Yat-sen (Zhongshan) University, Guangzhou 510275, People's Republic of China

[2]The Key Laboratory of Low-carbon Chemistry & Energy Conservation of Guangdong Province, Sun Yat-sen (Zhongshan) University, Guangzhou 510275, People's Republic of China

*Correspondence and requests for materials should be addressed to C. X. Wang

Tel & Fax: +86-20-84113901

E-mail: wchengx@mail.sysu.edu.cn

The synthesis of α-MnO_2 nanowires

The α-MnO_2 nanowires were prepared by a typical hydrothermal method. First, 3 mmol $KMnO_4$ was dissolved in 30 mL deionized water by magnetic stirring. Then, 1 mL HCl was added into the as-prepared solution and stirring continuously to form a homogeneous solution. Then, the solution was transformed into a 30 mL Teflon-lined stainless-steel autoclave and heated with a temperature of 140 ℃ for 12 hours. After cooling to room temperature, the products were collected by centrifugation, washed with water and ethanol several times, dried with 80 ℃ at the ambient condition overnight. The XRD pattern (Figure S15) and SEM images (Figure S16) confirmed the as-prepared products were α-MnO_2 nanowires.

The capacitive contribution calculation

The capacitive contributions can be obtained by integrating the CV curves at various sweep rates. The response current (i) at a fixed potential (V) is composed of two components: capacitive process ($k_1 v$) and diffusion process ($k_2 v^{1/2}$), which can be shown as the equation:

$$i(V)= k_1 v + k_2 v^{1/2} \qquad (1)$$

or

$$i(V)/v^{1/2}=k_1 v^{1/2}+k_2 \qquad (2)$$

Therefore, we can acquire the value of k_1 and k_2 by fitting the line of $i/v^{1/2}$ versus $v^{1/2}$. Then, the response current ($k_1 v$) resulted from the capacitive process can be calculated at every last potential. The capacitive contribution percentage can be calculated by convoluting the response current ($k_1 v$) and total response current (i).

The calculation of diffusion coefficients

The ion diffusion coefficients were acquired by GITT. The calculation method is based on the following equation:

$$D_{ion}= (4/\pi\tau)*[n_M V_M/S]^2[[\Delta E_S/\Delta E_t]^2 \qquad (3)$$

Where τ is the constant current pulse duration, n_M and V_M are the moles of $CaMn_3O_6$ and molar volume, respectively. S is the area of the electrode, and ΔE_s and ΔE_t are the change in the steady-state voltage and battery voltage.

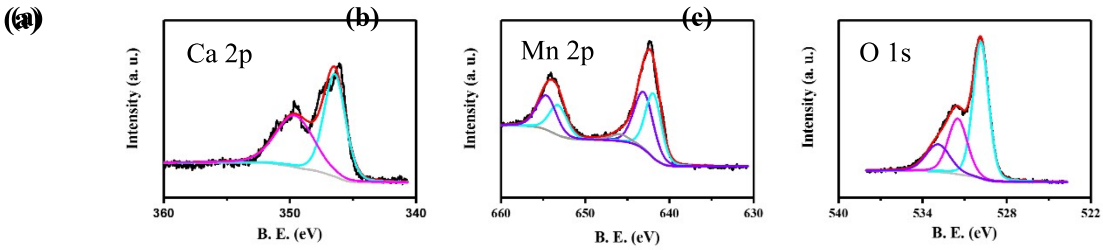

Figure S1 XPS spectra of CMO@EG. (a)Ca 2p; (b) Mn 2p; (c) O 1s.

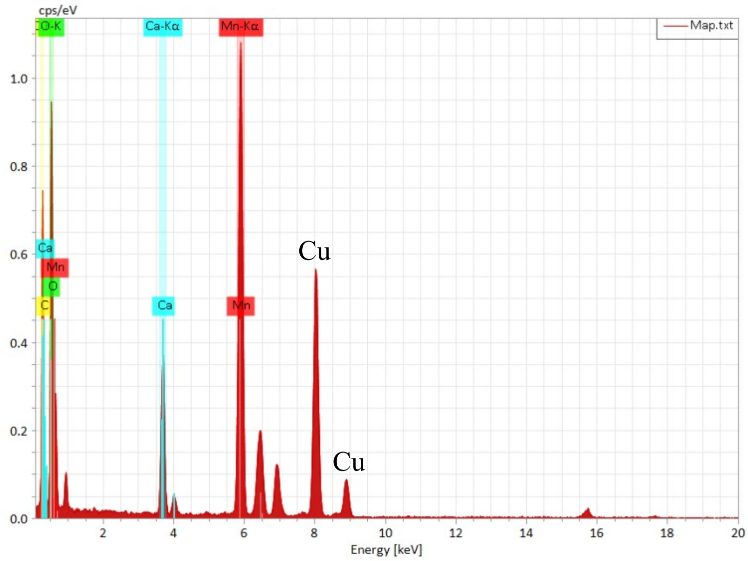

Figure S2 EDX spectra of CMO@EG composites.

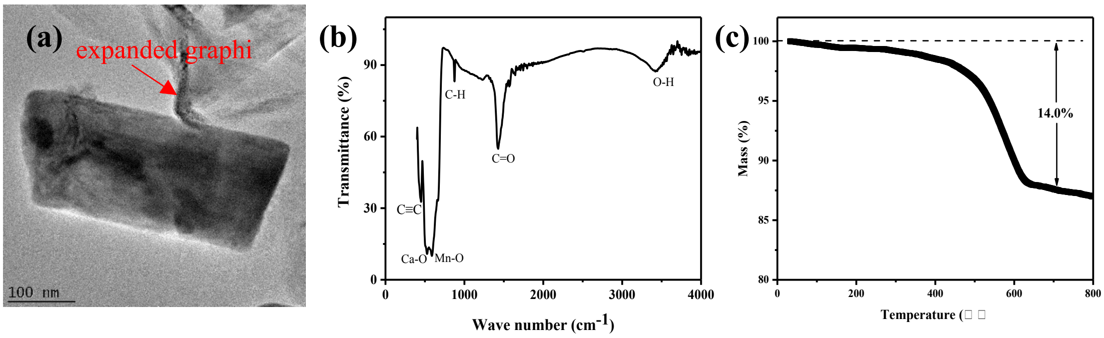

Figure S3. (a)TEM image of $CaMn_3O_6$@EG; (b) FT-IR curve; (c) TG curve.

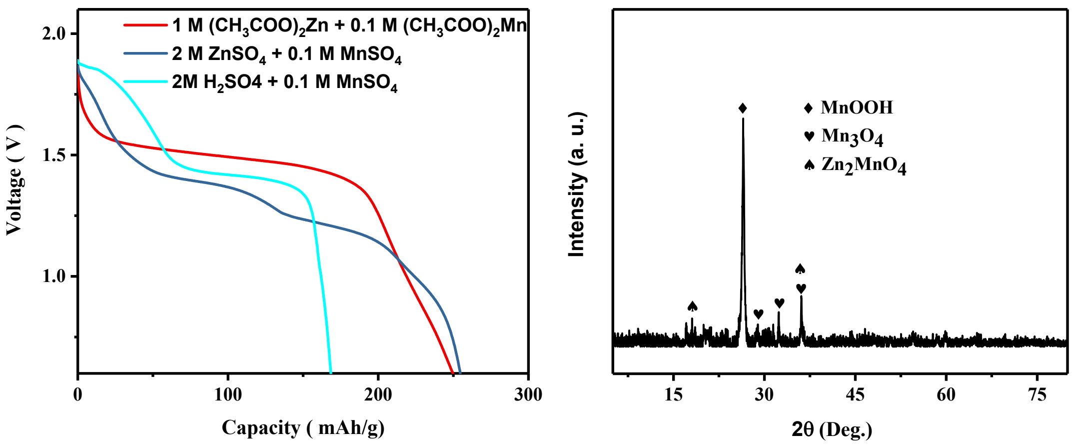

Figure S4 (a) Discharge curves of CMO electrode in different electrolytes; (b) the XRD pattern in 1 M $(CH_3COO)_2Zn$ + 0.1 M $(CH3COO)_2Mn$ at full discharge state.

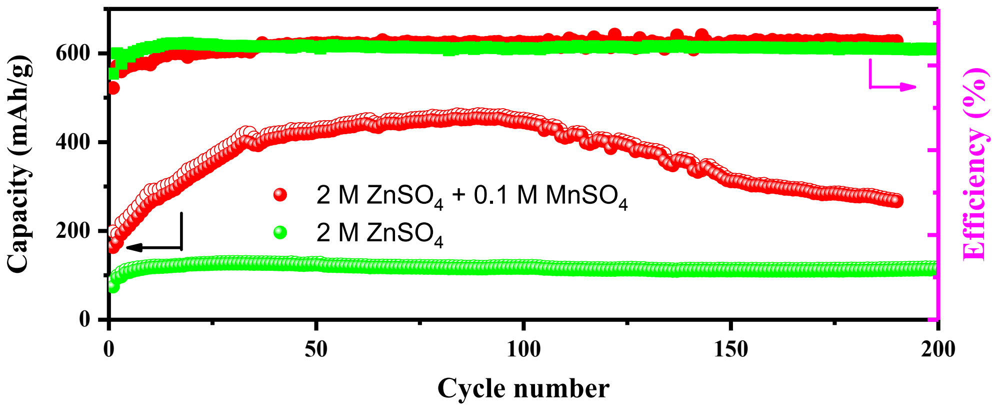

Figure S5 Cycling performance of CMO@EG cathode in 2 M $ZnSO_4$ and 2 M $ZnSO_4$ + 0.1 M $MnSO_4$ at 0.2 A/g, respectively.

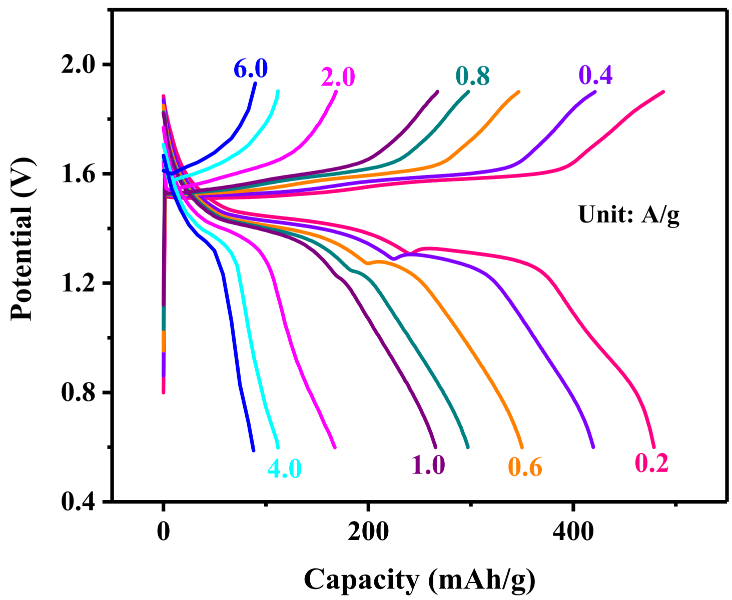

Figure S6 the GCD profiles of **α**-MnO_2 at different current densities from 0.2 to 6 A/g.

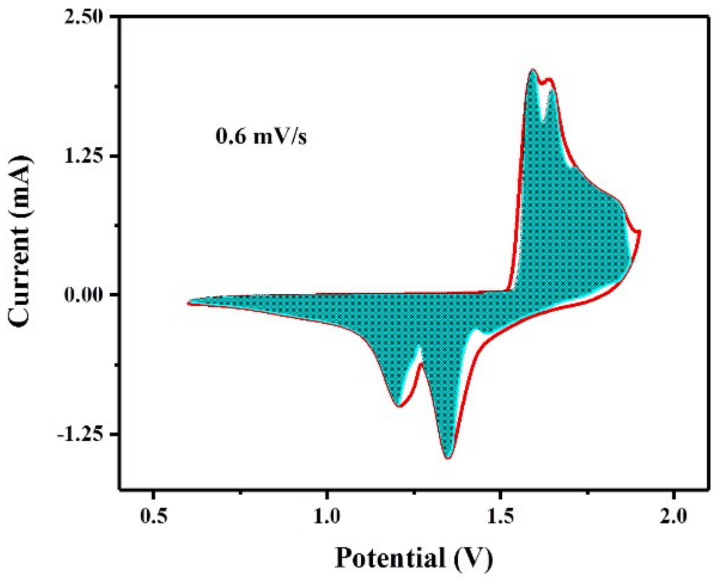

Figure S7 The corresponding capacitive contribution of CMO@EG cathode after 6 cycles at 0.6 mV/s

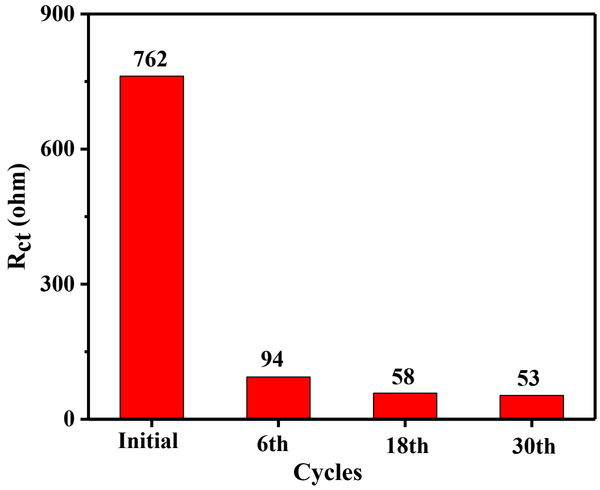

Figure S8 Comparsion of charge transfer resistance (R_{ct}) values of CMO@EG in different cycles (full charge), inset is the equivalent circuit applied for ESI fitting.

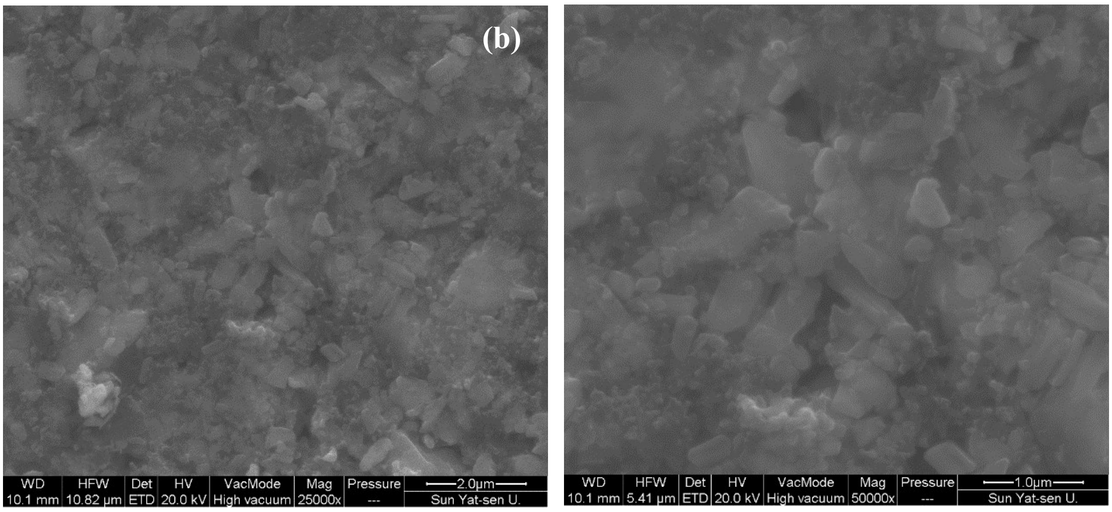

Figure S9 (a) and (b) SEM images of origin electrode.

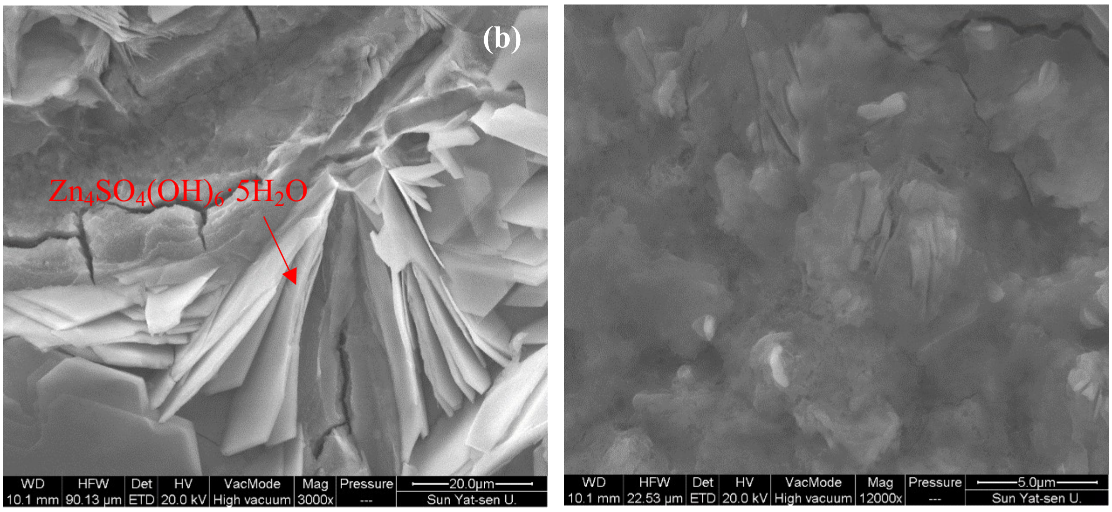

Figure S10 (a) and (b) SEM images of CMO@EG electrode at second full discharge state.

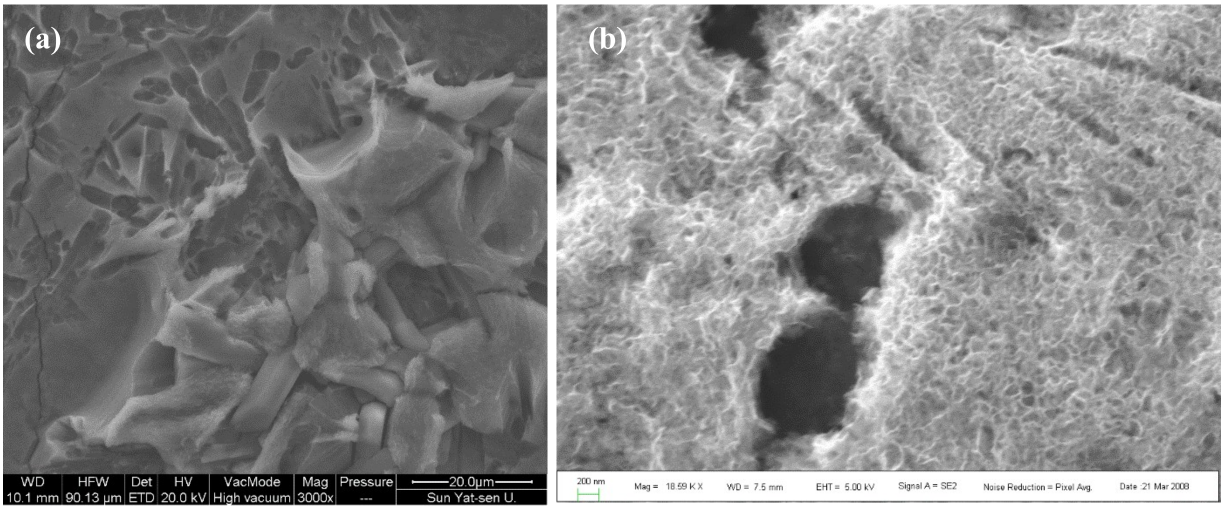

Figure S11 (a) and (b) SEM images of CMO@EG electrode at second full charge state.

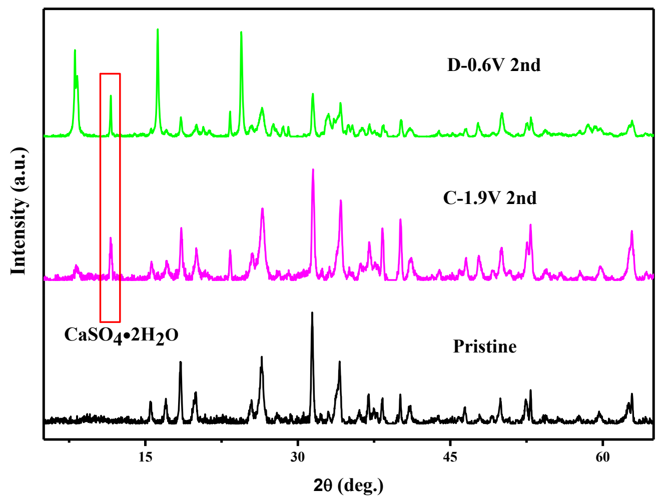

Figure S12. The XRD patterns of CMO@EG electrodes at different state at 2nd cycle.

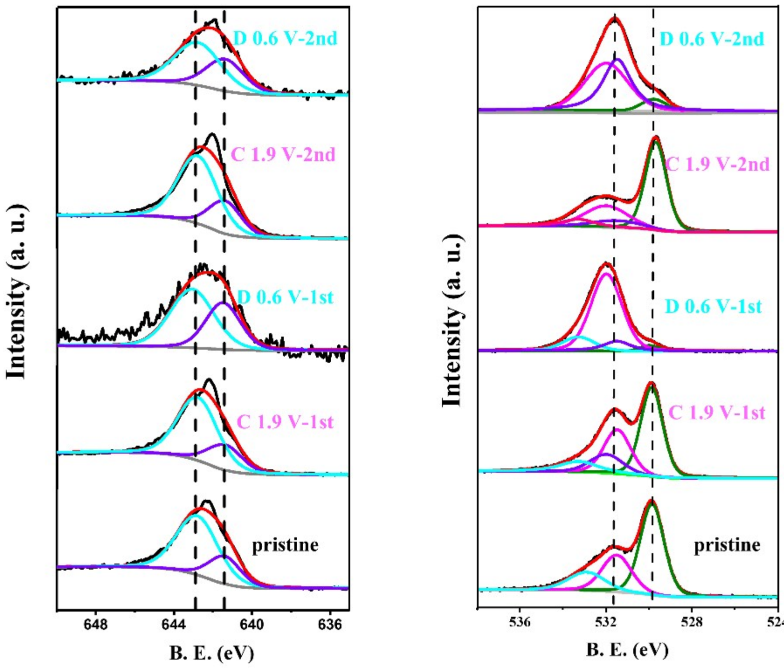

Figure S13 the *ex-situ* XPS spectra of origin, first full charge/discharge and second full charge/discharge states, (a) Mn $2p_{3/2}$, (b) O 1s.

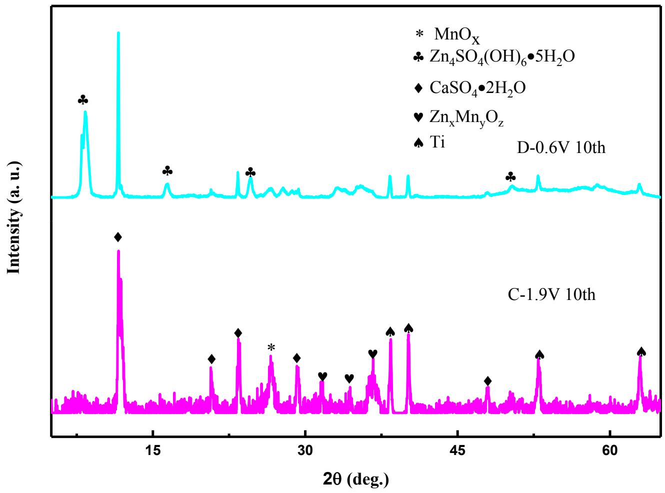

Figure S14. The XRD patterns of CMO@EG electrodes at different state at 10^{th} cycle.

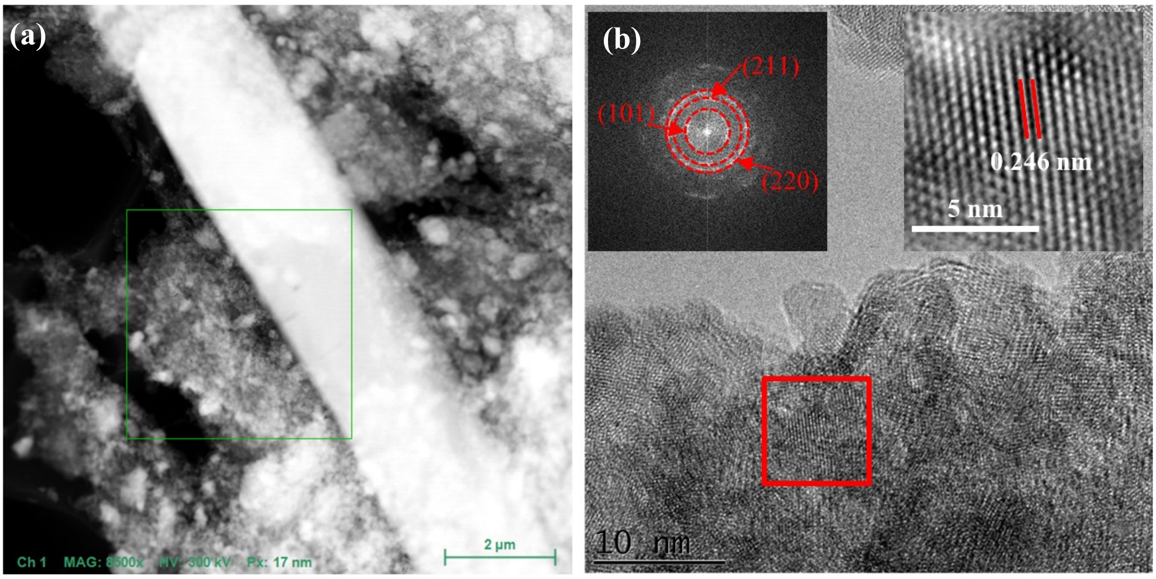

Figure S15 STEM image (a) and HRTEM image of CMO electrode at full charge state after 10 cycles

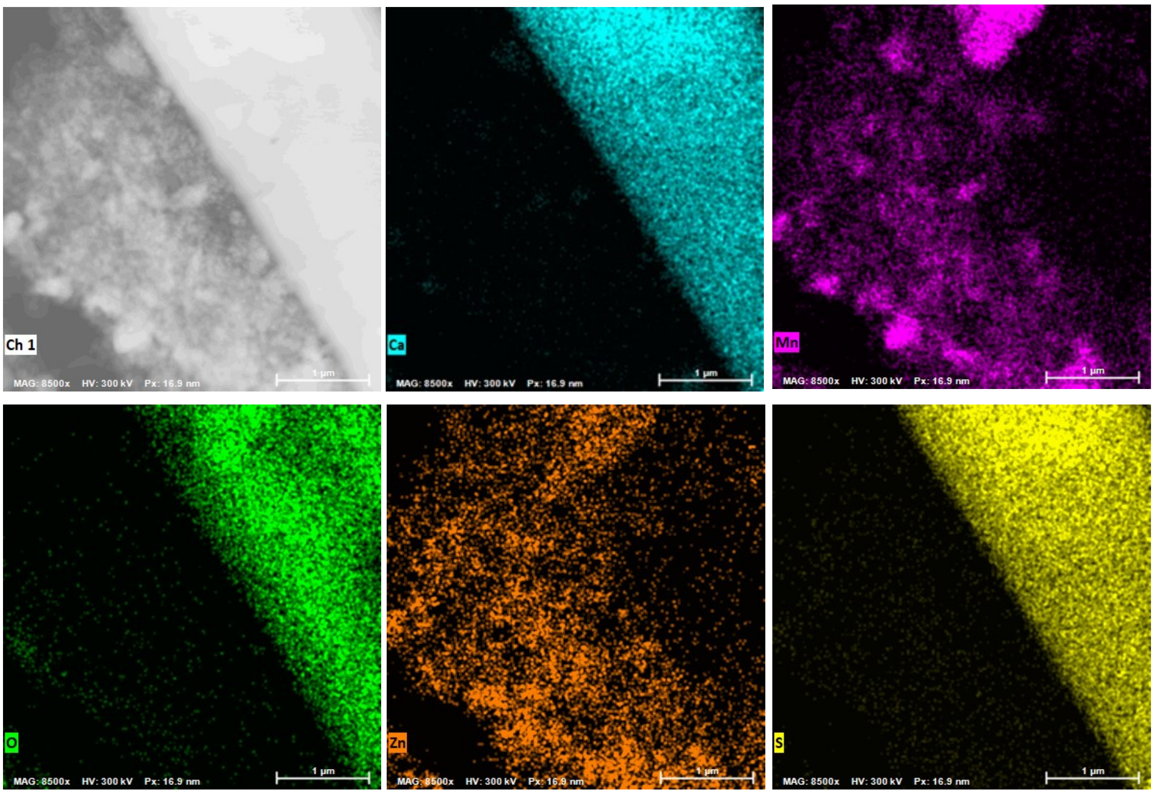

Figure S16 STEM-EDX images of CMO electrode at full charge state after 10 cycles

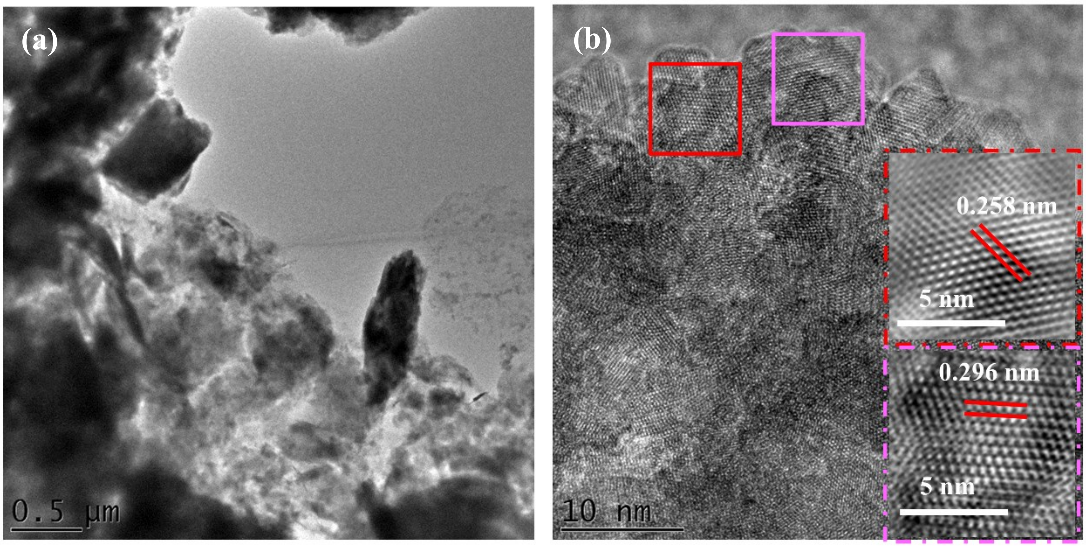

Figure S17 TEM image (a) and HRTEM image (b) of CMO electrode at full discharge state after 10 cycles

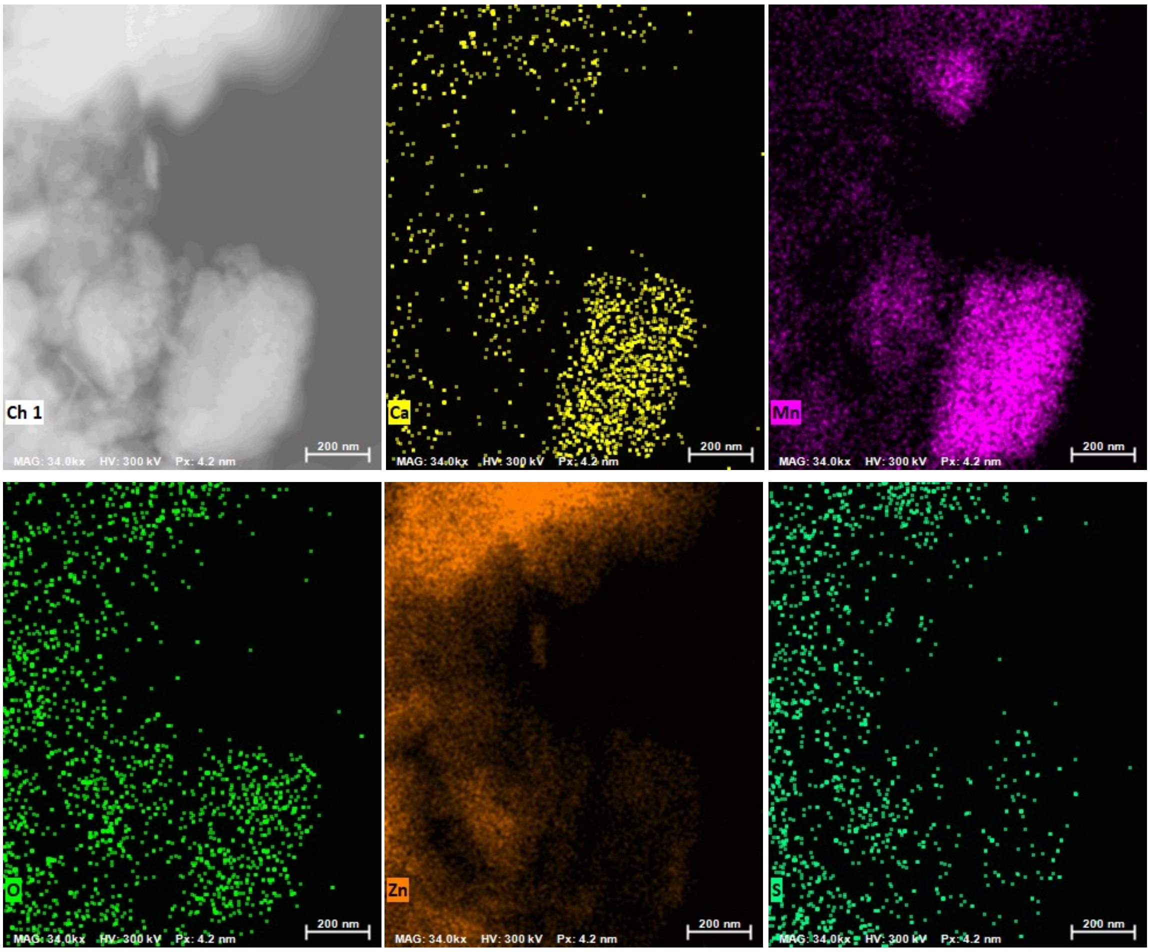

Figure S18 STEM-EDX images of CMO electrode at full charge state after 10 cycles

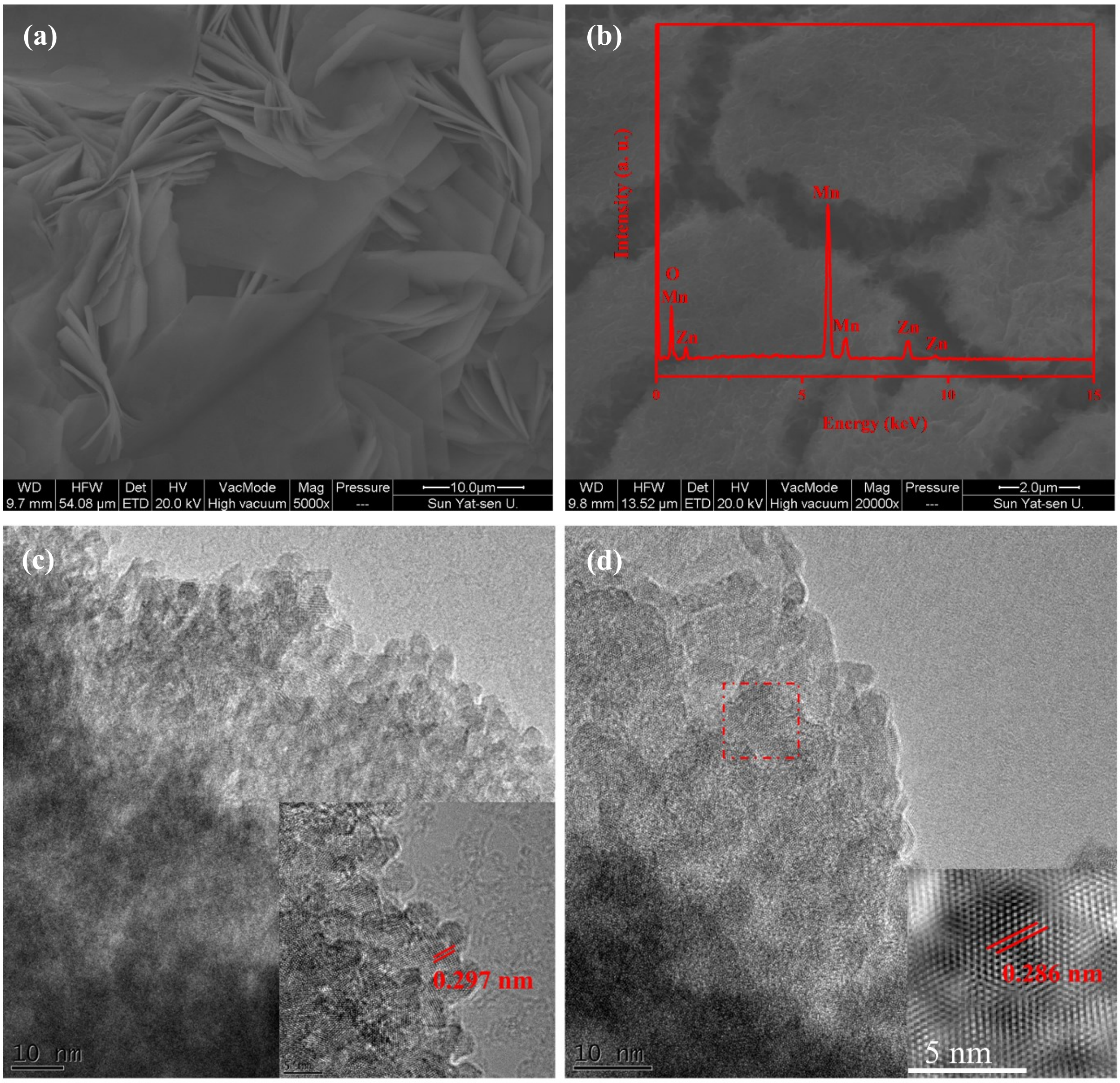

Figure S19 (a) and (c) SEM and TEM images of CMO electrode at full charge state after 100 cycles; (b) and (d) SEM images of CMO electrode at full charge state after 100 cycls, the inset of (b) is corresponding EDX spectrum.

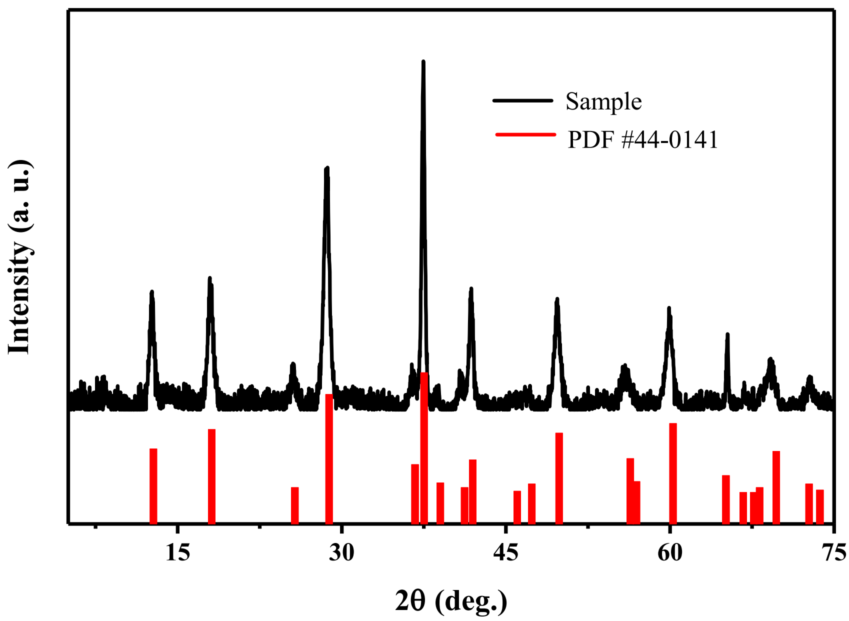

Figure S20 XRD pattern of α-MnO_2 nanowires.

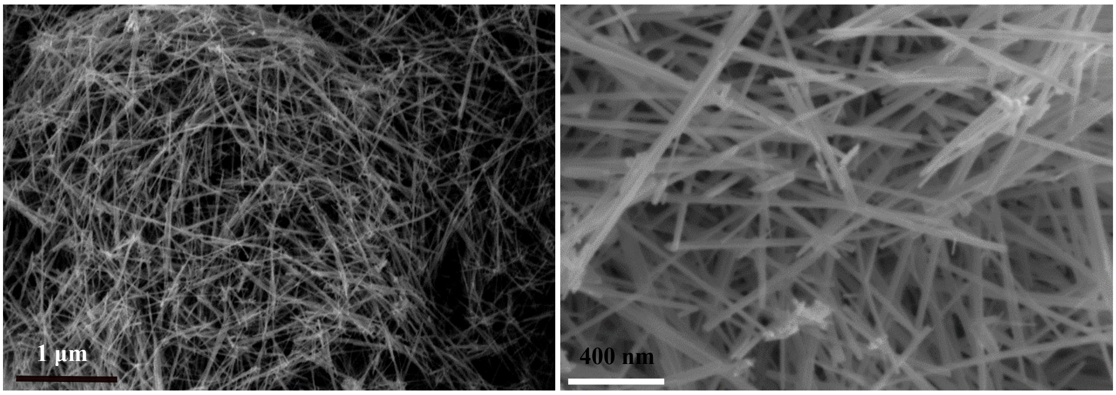

Figure S21 SEM images of α-MnO_2 nanowires.

Table S1 Comparison of the electrochemical performance of CMO@EG cathode with other reported Mn-based cathodes for AZIBs.

cathode	Voltage window	electrolyte	Specific capacity	Long-term performance	Ref.
MnS-EDO	0.8-2.0 V	2 M $ZnSO_4$ + 0.1 M $MnSO_4$	360 mAh/g at 0.3 A/g	104 mAh/g retained after 4000 cycles at 3.0 A/g	[1]
MnO@C	0.9 -1.8 V	2 M $ZnSO_4$+ 0.2 M $MnSO_4$	288 mAh/g at 0.1A/g	98% retained after 300 cycles at 0.5A/g	[2]
δ-MnO_2	1.0 -1.8 V	1 M $Zn(TFSI)_2$ + 0.1 M $Mn(TFSI)_2$	238 mAh/g at 0.2C	93% capacity retention after 4000 cycles at 20 C	[3]
Cation-Deficient $ZnMn_2O_4$	0.8 - 2.0 V	3M $Zn(CF_3SO_3)_2$	150 mAh/g at 50 mA/g	94 % retained after 500 cycles at 0.5A/g	[4]
oxygen-deficient MnO_2	1.0-1.8 V	1 M $ZnSO_4$ + 0.2 M $MnSO_4$	345 mAh/g at 0.2 A/g.	94% capacity retention after 100 cycles at 0.2A/g	[5]
$K_{0.8}Mn_8O_{16}$	0.8-1.8 V	2 M $ZnSO_4$ + 0.1 M $MnSO_4$	320 mAh/g at 0.1A/g	1000 cycles with no obvious capacity fading at 1A/g	[6]
$K_{1.33}Mn_8O_{16}$	1.0 -1.8 V	2 M $ZnSO_4$ + 0.1 M $MnSO_4$	312 mAh/g at C/10	more than 80% of initial capacity after 650 cycles at 5C	[7]
Ni^{2+} doping Mn_2O_3	0.8-1.8 V	2 M $ZnSO_4$	252 mAh/g at 0.1 A/g	≈85.6% over 2500 cycles at 1.0 A/g	[8]
Superfine MnO_2 nanowires	1.0-1.9 V	2 M $ZnSO_4$ + 0.1 M $MnSO_4$	388 mAh/g at 0.6 A/g	negligible deterioration after 1000 cycling tests at 1.0 A/g	[9]
Co doping Mn_3O_4	0.2-2.2 V	2 M $ZnSO_4$ + 0.2 M $MnSO_4$	362 mAh/g at 0.1 A/g	80% retention after 1100 cycles at 2.0A/g	[10]
O_d-Mn_3O_4 @C NA/CC	0.2-1.85 V	2 M $ZnSO_4$ + 0.2 M $MnSO_4$	396.2 mAh/g at 0.2 A/g	95.7% of the initial capacity after 12000 cycles at 5A/g	[11]
Mg_2MnO_4	0.4-1.9 V	2 M $ZnSO_4$ + 0.1 M $MnSO_4$	371.7 mAh/g at 0.15A/g	no obvious capacity fading after 2000 cycles at 3 A/g	[12]
$K_{0.28}MnO_2\cdot0.1H_2O$	0.4-1.9 V	3M $ZnSO_4$ + 0.2M $MnSO_4$	300 mAh/g at 0.1A/g	95% capacity retention after 1000 cycles at 2 A/g	[13]
$LiMn_2O_4$	0.8-1.9 V	1 M $ZnSO_4$+ 1 M Li_2SO_4+ 0.1 M $MnSO_4$	300 mAh/g at 0.1 A/g	93.5% retention after 1500 cycls at 1A/g	[14]

δ-MnO2	0-2.0 V	2 M ZnSO4 + 0.1 M MnSO4	330 mAh/g at 1.5 mA/cm^2	100% capacity retention after 6000 cycles at 5 mA/ cm2.	[15]
$Ca_{0.28}MnO_2 \cdot 0.5H_2O$	0.4-1.9 V	1 M $ZnSO_4$ + 0.1 M MnSO4	298 mAh/g at 0.175A/g	5000 cycles with no obvious capacity fading	[16]
SSWM@Mn_3O_4	1.0-1.8 V	2 M $ZnSO_4$ + 0.1M $MnSO_4$	296 mAh/g at 0.1A/g	500 cycles at 0.5A/g	[17]
Mn-defect MnO	0.8-1.8 V	2 M $ZnSO_4$ + 0.1 M $MnSO_4$	300 mAh/g at 0.1 A/g	116 mAh/g at 1 A/g after 1500 cycles.	[18]
Ca_2MnO_4	0.8-1.8 V	2 M $ZnSO_4$ + 0.1 M $MnSO_4$	250 mAh/g at 0.1 A/g	no obvious fluctuation for 1000 cycles at 1A/g	[19]
6.0 Nanometer SpinelNanodot	0.9-1.9 V	2 M $ZnSO_4$ + 0.2 M $MnSO_4$	386.7 mAh/g at 0.1 A/g	500 cycles at 0.5 A/g	[20]
α-MnO_2	0.8-1.8 V	2 M $ZnSO_4$ + 0.1 M $MnSO_4$ in palygorskite	290 mAh/g at 0.2 A/g	100% retention after 1000 cycles at 1 A/g	[21]
CMO@EG	0.6-1.9 V	2 M $ZnSO_4$+ 0.1 M $MnSO_4$	521.7 mAh/g at 0.2 A/g	100% capacity retention after 2350 cycles at 2A/g, 75% after extra 17000 cycles at 5A/g	This work

Reference

[1]. X. J. Chen, W. Li, Y. B. Xu, et al., Charging Activation and Desulfurization of MnS Unlock the Active Sites and Electrochemical Reactivity for Zn-Ion Batteries. *Nano Energy*, 2020. **75**, 104869.

[2]. W. J. Li, X. Gao, Z. Y. Chen, et al., Electrochemically activated MnO cathodes for high performance aqueous zinc-ion battery. Chemical Engineering Journal, 2020. **402**(15),125509.

[3]. Y. Jin, L. F. Zou, L. L. Liu, et al., Joint Charge Storage for High‐Rate Aqueous Zinc–Manganese Dioxide Batteries. *Advanced Materials*, 2019. **31**(29), 1900567.

[4]. N. Zhang, F. Y. Cheng, Y. C. Liu, et al., Cation-Deficient Spinel $ZnMn_2O_4$ Cathode in $Zn(CF_3SO_3)_2$ Electrolyte for Rechargeable Aqueous Zn-Ion Battery. *Journal of the American Chemical Society*, 2016. **138**(39), 12894-12901.

[5]. T. Xiong, Z. G. Yu, H. J. Wu, et al., Defect Engineering of Oxygen-Deficient Manganese Oxide to Achieve High-Performing Aqueous Zinc Ion Battery. *Advanced Energy Materials*, 2019. **9**(14), 1803815.

[6]. G. Z. Fang, C. Y. Zhu, M. H. Chen, et al., Suppressing Manganese Dissolution in Potassium Manganate with Rich Oxygen Defects Engaged High-Energy-Density and Durable Aqueous Zinc-Ion Battery. *Advanced Functional Materials*, 2019. **29**(15), 1808375.

[7]. K. Sada, B. Senthilkumar, and P. Barpanda, Cryptomelane $K_{1.33}Mn_8O_{16}$ as a Cathode for Rechargeable Aqueous Zinc-ion Batteries. *Journal of Materials Chemistry A*, 2019. **7**(41), 23981-23988.

[8]. D. D. Zhang, J. Gao, X. Y. Zhang, et al., Inhibition of Manganese Dissolution in Mn_2O_3Cathode with Controllable Ni^{2+}Incorporation for High‐Performance Zinc Ion Battery. A*dvanced Functional Materials*, 2021. **31**(14), 2009412.

[9]. J. J. Wang, J. G. Wang, X. P. Qin, et al., Superfine MnO_2 Nanowires with Rich Defects toward Boosted Zinc Ion Storage Performance. *ACS Applied Materials & Interfaces*, 2020. **12**(31), 34949-34958.

[10]. J. Ji, H. Z. Wan, B. Zhang, et al., $Co^{2+/3+/4+}$-Regulated Electron State of Mn-O for Superb Aqueous Zinc-Manganese Oxide Batteries. *Advanced Energy Materials*, 2021. **11**(6), 2003203.

[11]. Q. Y. Tan, X. T. Li, B. Zhang, et al., Valence Engineering via In Situ Carbon Reduction on Octahedron Sites Mn_3O_4 for Ultra-Long Cycle Life Aqueous Zn-Ion Battery. Advanced Energy Materials, 2020. **10**(38), 2001050.

[12]. X. M. Yuan, T. J. Sun, S. B. Zheng, et al., An inverse-spinel Mg_2MnO_4 cathode for high-performance and flexible aqueous zinc-ion batteries. *Journal of Materials Chemistry A*, 2020. **8**(43), 22686-22693.

[13]. Y. D. Jiao, L. Q. Kang, J. B. Gair, et al., Enabling stable MnO_2 matrix for aqueous zinc-ion battery cathodes. *Journal of Materials Chemistry A*, 2020. **8**(42), 22075-22082.

[14]. T. S. Zhang, Y. Tang, G. Z. Fang, et al., Electrochemical Activation of

Manganese-Based Cathode in Aqueous Zinc-Ion Electrolyte. *Advanced Functional Materials*, 2020 **30**(30) 2002711.

[15]. Y. Q. Jiang, D. L. Ba, Y. Y. Li, et al., Noninterference Revealing of "Layered to Layered" Zinc Storage Mechanism of δ-MnO_2 toward Neutral Zn–Mn Batteries with Superior Performance. *Advanced Science*, 2020. **7**(6), 1902795.

[16]. T. J. Sun, Q. S. Nian, S. B. Zheng, et al., Layered $Ca_{0.28}MnO_2 \cdot 0.5H_2O$ as a High Performance Cathode for Aqueous Zinc-Ion Battery. Small.16(17), 2000597.

[17]. C. Y. Zhu, G. Z. Fang, J. Zhou, et al., Binder-free stainless steel@Mn_3O_4 nanoflower composite: a high-activity aqueous zinc-ion battery cathode with high-capacity and long-cycle-life. *Journal of Materials Chemistry A*, 2018. **6**(20), 9677-9683.

[18]. C. Y. Zhu, G. Z. Fang, S. Q. Liang, et al., Electrochemically Induced Cationic Defect in MnO Intercalation Cathode for Aqueous Zinc-ion Battery. *Energy Storage Materials*, 2020. **24**, 394-401.

[19]. S. Guo, S. Q. Liang, B. S. Zhang, et al., Cathode Interfacial Layer Formation via in Situ Electrochemically Charging in Aqueous Zinc-Ion Battery. *ACS Nano*, 2019. **13**(11), 13456-13464.

[20]. L. Jiang, Z. Y. Wu, Y. Wang, et al., Ultrafast Zinc-Ion Diffusion Ability Observed in 6.0-Nanometer Spinel Nanodots. ACS Nano, 2019. **13**(9), 10376-10385.

[21]. J. W. Gao, X. S. Xie, S. Q. Liang, et al., Inorganic Colloidal Electrolyte for Highly Robust Zinc-Ion Batteries. Nano-Micro Letters, 2021. 13, 69.